Japanese Journal of Applied Physics
Vol. 45, No. 5B, 2006, pp. 4313–4320

Review Paper

©2006 The Japan Society of Applied Physics

Crystallization of Si in Millisecond Time Domain Induced by Thermal Plasma Jet Irradiation

Seiichiro HIGASHI*, Hirotaka KAKU, Tatsuya OKADA, Hideki MURAKAMI and Seiichi MIYAZAKI

Department of Semiconductor Electronics and Integration Science, Graduate School of Advanced Sciences of Matter, Hiroshima University, 1-3-1 Kagamiyama, Higashi-Hiroshima, Hiroshima 739-8530, Japan

(Received August 6, 2005; revised January 26, 2006; accepted February 7, 2006; published online May 25, 2006)

Investigations on the temperature profiles and formation of crystalline Si in rapid thermal annealing induced by thermal plasma jet (TPJ) irradiation have been reviewed. Substrate surface temperature during annealing has been measured by an optical probe method which has an accuracy of 30 K and a time resolution of millisecond. By changing the annealing conditions such as scan speed (v), plasma–substrate gap (d) and Ar gas flow rate (f), maximum surface temperature (T_{max}) is controlled in the ranges of 960 to 1860 K with a typical annealing duration (t_a) of $\sim$3 ms. On the basis of temperature measurement and *in-situ* reflectivity measurement techniques, the phase transformation of amorphous Si (a-Si) films has been investigated. When the a-Si films are heated to a temperature higher than the melting point, solid phase crystallization (SPC) followed by melting and resolidification of the films have been observed. It was found that SPC temperature increased from 1096 to 1284 K with decreasing crystallization time from 1.4 to 0.12 ms. Thin-film transistors (TFTs) fabricated using the SPC films show good electrical characteristics with an average field effect mobility of 61 $cm^2 \cdot V^{-1} \cdot s^{-1}$ and a threshold voltage of 3.4 V. By annealing SiO_x films at temperatures higher than 1430 K using a TPJ, the precipitation of nanocrystalline Si with a size ranging from 10 to 250 nm has been observed. [DOI: 10.1143/JJAP.45.4313]

KEYWORDS: thermal plasma jet, rapid thermal annealing, phase transformation, thin-film transistor, nanocrystal

1. Introduction

Rapid thermal annealing under nonequilibrium condition is one of the key process technologies for the fabrication of large area electronic devices such as thin-film transistors (TFTs) and solar cells. By localizing the heat to the substrate surface, amorphous Si (a-Si) films are crystallized without serious thermal damage to the substrates, which allow the use of low heat-resistant substrates such as glass and plastic. There are a variety of rapid thermal annealing techniques with time domain ranging from nano- to microsecond. In the case of excimer laser annealing (ELA), nanosecond laser light with peak power density as high as 10 MW/cm^2 is used to heat a-Si films to a temperature higher than the melting point.[1,2] The CW laser scanning[3–8] and the Joule heating[9–11] techniques are performed to crystallize a-Si films in microsecond time domain with power density ranging from 100 kW/cm^2 to 1 MW/cm^2. In the nano- and microsecond annealing techniques, laser is frequently used because one can easily obtain high power density by simply focusing the light with a lens. However, the output power of laser is limited and the application of laser annealing techniques to large area processing results in an increase in production cost. If one pays attention to millisecond time domain, the required power density to heat the a-Si films to a temperature higher than the crystallization temperature is in the range of several 10 kW/cm^2, which is much lower than those of previous cases, and this result gives us the opportunity to implement a new heat source for the annealing.

Recently, we have developed a millisecond annealing technique using thermal plasma jet (TPJ).[12,13] This is an atmospheric pressure process utilizing a DC arc discharge thermal plasma which can generate high power using a simple equipment structure. Because thermal plasma has a high density on the order of 10^{18} cm^{-3} with a temperature higher than 10000 K,[14] the electrical power introduced in the plasma is strongly concentrated. The plasma jet transfers the power to the substrate surface. In this study, the temporal variation in substrate surface temperature induced by thermal plasma jet irradiation is investigated using a noncontact temperature measurement technique. The applications of the annealing technique to the crystallization of a-Si films and the formation of nanocrystalline Si have been investigated.

2. Experimental

The thermal plasma source used in the experiment is schematically shown in Fig. 1. The W cathode and the water-cooled Cu anode separated 1 to 2 mm from each other were connected to a power supply. Arc discharge was generated by supplying DC power (p) of 1.57 to 2.62 kW, where DC voltage and current range from 12.3 to 15.3 V and from 130 to 200 A, respectively, between the electrodes under an Ar gas flow rate (f) of 4.2 to 9.8 L/min. The TPJ was formed by blowing out the arc plasma through an orifice of 3 to 4 mm in diameter. The substrate was linearly moved by a motion stage in front of the plasma jet with scanning speed (v) ranging from 170 to 1200 mm/s. The distance between the plasma source and the substrate (plasma–substrate gap d) was varied from 0.8 to 5 mm. To measure the temperature profile generated in the quartz substrate during the TPJ irradiation, transient reflectivity was measured by irradiating the substrate with a laser light ($\lambda = 633$ or 532 nm) from the backside and detecting the reflected light intensity using a photodiode through a band pass filter [see Fig. 1(A)]. For the observation of the phase transformation of the a-Si films that were deposited on the quartz substrate by plasma-enhanced chemical vapor deposition (PECVD), the transient reflectivity of the films were measured using a similar apparatus [see Fig. 1(B)]. Because the refractive index of Si is 4.5–4.8 in the amorphous phase and is 3.9–4.1 in the crystalline phase ($\lambda = 532$–633 nm), one can observe phase transformation from the transient variation in the Si film's reflectivity in the beam path (B). The reflected light intensity from an Al evaporated quartz substrate was used as the reference for the absolute

*E-mail address: sehiga@hiroshima-u.ac.jp

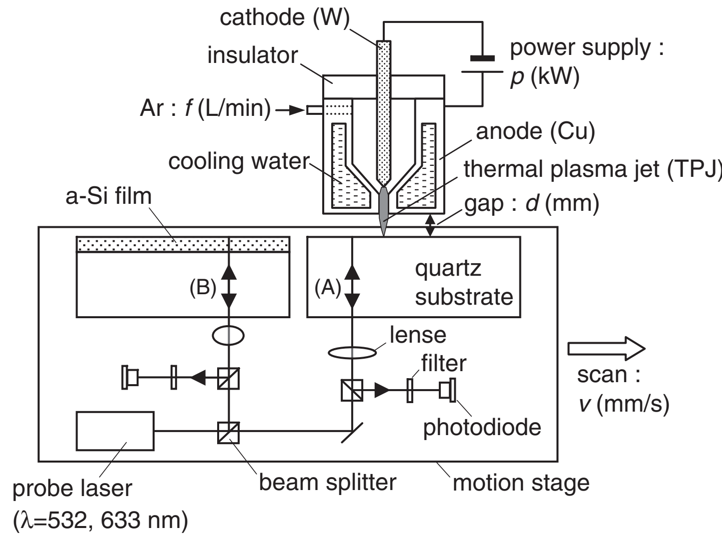

Fig. 1. Schematic diagram of experimental setup for millisecond annealing using thermal plasma jet (TPJ). Annealing experiments are performed by varying power input to plasma source p (kW), Ar gas flow rate f (L/min), plasma–substrate gap d (mm) and scan speed v (mm/s). The optics behind the substrates are used (A) to measure temperature profile in a quartz substrate and (B) to observe the phase transformation of a-Si films during the TPJ irradiation.

reflectivity calculation. The measurement system was set on a motion stage and moved together with the specimen in front of the TPJ as shown in Fig. 1. By performing the transient reflectivity measurements using the beam paths (A) and (B) simultaneously, the temperature of phase transformation was precisely determined as discussed in §4.1.

3. Noncontact Measurement of Transient Temperature Profile

We observed the oscillating transient reflectivity of He–Ne laser light ($\lambda = 633$ nm) in beam path (A) during the plasma jet irradiation and an example is shown by the solid line in Fig. 2(a). The number of oscillation increases with decreasing v, which suggests that the increase in the number of oscillation reflects an increasing surface temperature. The oscillation in the transient reflectivity is due to the interference of the incident light multiply reflected between the top and bottom surfaces of the substrate as schematically shown in the inset of Fig. 2(a). Because the refractive index of quartz (n_Q) changes with temperature [$n_Q = 1.457 + 1.27 \times 10^{-5} \times T$ (°C)],[15] the optical thickness of the quartz substrate during the annealing changes and this induces the oscillation in the reflected laser light. By analyzing the change in optical thickness, we can obtain temporal variation in temperature profile. The analysis is performed by the following steps.[16] First, two-dimensional heat flow simulation is performed on the basis of the following equation.

$$\frac{\partial T(x,y)}{\partial t} = \frac{\kappa}{\rho c}\left(\frac{\partial^2 T(x,y)}{\partial x^2} + \frac{\partial^2 T(x,y)}{\partial y^2}\right) + \frac{S}{\rho c}, \qquad (1)$$

where x is the position along the plasma jet scanning direction, y is the depth from the substrate surface, T is the temperature, t is the time, κ, ρ, and c are the thermal conductivity, the density and the specific heat of the quartz substrate, respectively, and S is the thermal incidence. Numerical calculation is performed by an explicit method with the following boundary conditions: that the side edges

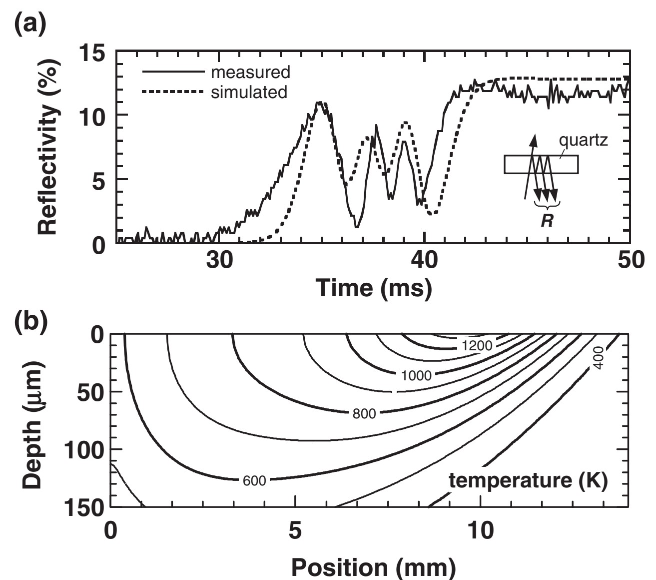

Fig. 2. (a) Comparison of transient reflectivity waveforms measured (solid line) and simulated (dotted line), and (b) temperature profile generated in quartz substrate obtained by analysis. The horizontal and vertical axes in (b) indicate the position along the TPJ scan direction and depth from the surface, respectively. The annealing conditions are as follows: a p of 2.24 kW, an f of 9.8 L/min, a d of 3.0 mm, and a v of 700 mm/s.

of the substrate are thermally insulated, and that the initial temperature is 300 K. It is assumed that the TPJ has a two-dimensional double Gaussian power profile with the width of W, and the effective power transfer efficiency from plasma to the substrate surface of η. Then, optical reflectivity simulation was performed based on the temperature profile at each time considering the temperature dependence of n_Q, multiple reflections and the interference effect of the laser light. The simulated transient reflectivity is compared with the experimental one and the fitting parameters W and η are optimized until the best fitting is obtained as shown by a

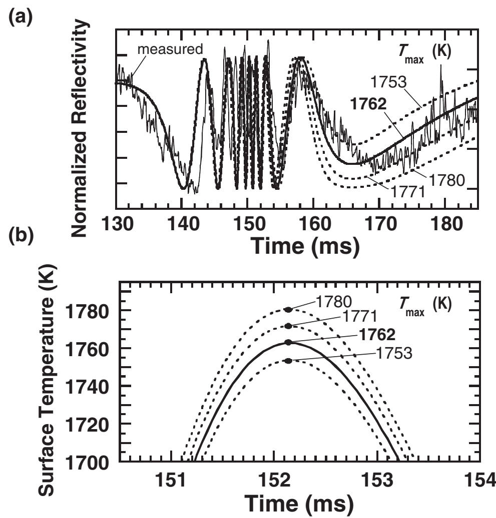

Fig. 3. (a) Comparison of transient reflectivity between experiment (noisy solid line) and simulation (smooth solid line and dotted lines). Transient reflectivity waveforms simulated under slightly different η values are superimposed in the graph to confirm the fitting accuracy; (b) shows surface temperature profile obtained under each η value.

dotted line in Fig. 2(a). Accordingly, we can obtain the most probable transient temperature profiles as an example is shown in Fig. 2(b). In this figure, the center of the plasma jet running with 700 mm/s to the positive direction is located at 10.5 mm in the horizontal axis where the position of surface maximum temperature (1344 K) is 1.0 mm behind ($x = 9.5$ mm). Temperature rapidly decreases with depth (vertical axis) as shown in Fig. 2(b) because the characteristic heat diffusion length in quartz is several 10 μm in millisecond annealing (~70 μm in the present case).

The accuracy of the measurement has been evaluated in terms of errors in fitting and absolute temperatures.[17] To evaluate fitting accuracy, the simulated reflectivity and corresponding temperature profiles under slightly different η values are shown in Figs. 3(a) and 3(b), respectively. By changing η with an increment of 1.2%, the maximum surface temperature (T_{max}) changes roughly by 10 K as shown in Fig. 3(b), and the corresponding variation in optical reflectivity is more than 10% as shown in Fig. 3(a). This result indicates that transient reflectivity sensitively detects a small variation in temperature. In this example, we determined the thick solid line ($T_{max} = 1762$ K) to be the best fitting to the experimental waveform. Even in the cases wherein higher or lower lines (dotted lines) are chosen, the difference in T_{max} is within 30 K. From this result, we can conclude that the error in the fitting procedure is less than 30 K. For the evaluation of error in absolute temperature, the melting point of the Si film was measured; the experimental details will be explained in §4.1. An example is shown in Fig. 6(b), where we measured the melting point of Si to be 1660 K. Because we know that the melting point of Si is 1687 K, this result indicates that the temperature accuracy is also within 30 K. From these results, we conclude that the accuracy of this temperature measurement is 30 K.

On the basis of this temperature measurement technique, we have evaluated surface temperature under various TPJ annealing conditions. First, the temperature measurement was performed at different v values and several examples are

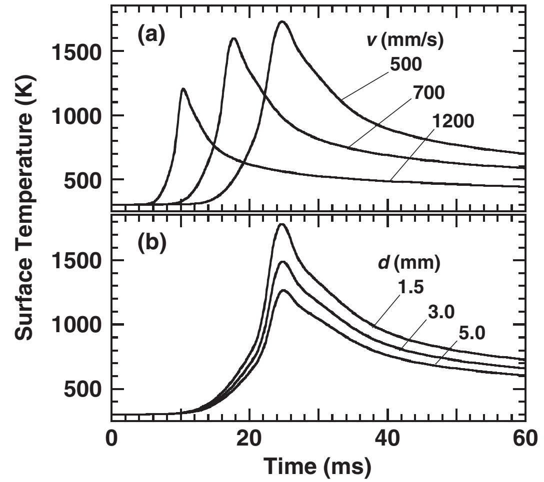

Fig. 4. Transient variations in substrate surface temperature obtained by noncontact measurement technique. (a) shows the results under different v values with a constant p of 2.10 kW, an f of 9.8 L/min, and a d of 3.0 mm, whereas (b) shows the results under different d values with a constant p of 2.15 kW, an f of 9.8 L/min, and a v of 500 mm/s.

Table I. Characteristic values of TPJ annealing performed under different v values and constant p of 2.10 kW, f of 9.8 L/min and d of 3.0 mm.

v (mm/s)	500	700	1200
T_{max} (K)	1726	1595	1201
t_a (ms)	2.8	2.0	1.2
R_h ($\times 10^5$ K/s)	3.50	4.51	5.31
R_c ($\times 10^5$ K/s)	1.21	1.48	1.61

Table II. Characteristic values of TPJ annealing performed under different d values and constant p of 2.15 kW, f of 9.8 L/min and v of 500 mm/s.

d (mm)	1.5	3.0	5.0
T_{max} (K)	1781	1488	1266
t_a (ms)	2.6	2.8	3.0
R_h ($\times 10^5$ K/s)	3.87	2.93	2.23
R_c ($\times 10^5$ K/s)	1.47	1.00	0.69

shown in Fig. 4(a). T_{max}, annealing duration (t_a), maximum heating rate (R_h) and cooling rate (R_c) extracted from these results are shown in Table I. Here, we define t_a to be the period during which surface temperature exceeds the 90% of the T_{max}. By changing v, both T_{max} and t_a vary simultaneously. The measured T_{max} and t_a as functions of v are plotted in Fig. 5(a). By changing v in the range of 500 to 1200 mm/s, both T_{max} and t_a change in the ranges of 1200 to 1730 K and 1.2 to 2.8 ms, respectively. The result is simply explained by an increase in thermal energy transfer from the TPJ to the surface at a low v. As for the next step, the d dependence of surface temperature was examined at a constant $v = 500$ mm/s and several examples are shown in Fig. 4(b). T_{max}, t_a, R_h, and R_c are summarized in Table II. Obviously, T_{max} increases with decreasing d, however, t_a seemingly remains almost unchanged in contrast to the case of Fig. 4(a). The measured T_{max} and t_a as functions of d under different f values of 4.2 and 9.8 L/min are shown in Fig. 5(b). We have found that T_{max} can be controlled in the range of ~960 to ~1780 K. Note that t_a remains almost unchanged at approximately 3 ms by annealing the sample at a constant v. This result indicates that T_{max} and t_a are

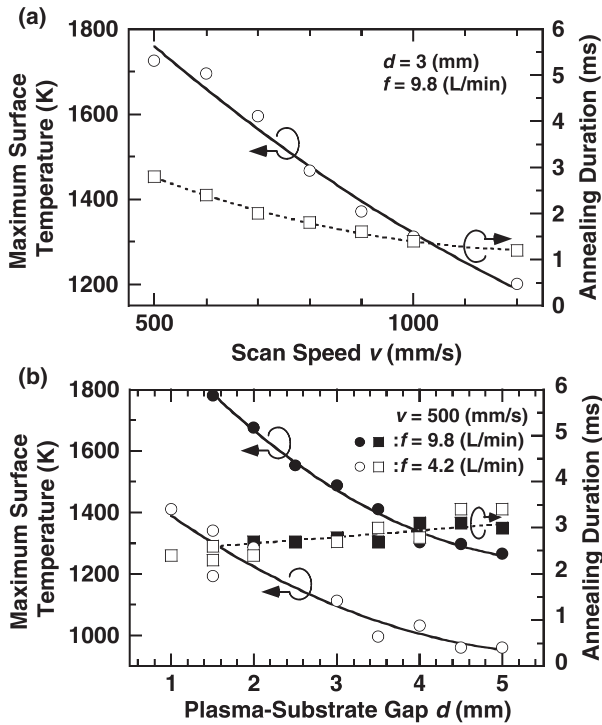

Fig. 5. Extracted T_{max} and t_a as functions of (a) v and (b) d. p was fixed at 2.10 kW in (a) and 2.15 kW in (b). The results obtained when f values are changed from 4.2 to 9.8 L/min are also shown in (b).

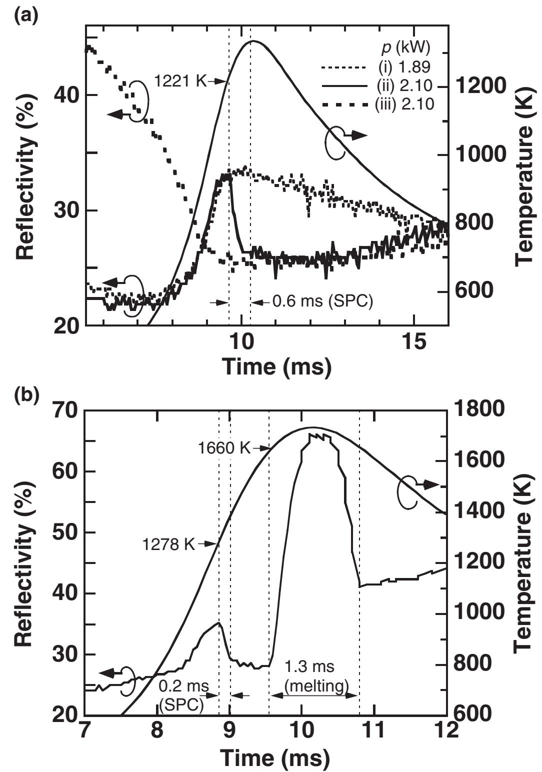

Fig. 6. Transient reflectivity waveforms and surface temperature profile obtained under sets of conditions of (a) d of 3.3 mm, v of 770 mm/s, f of 7.0 L/min with different p values from 1.89 to 2.10 kW and (b) v of 770 mm/s, d of 0.8 mm, f of 7.0 L/min, and p of 2.10 kW. The vertical dashed lines in the figure indicate the duration of SPC and the melting of Si films.

controlled independently by changing d, f, and v, respectively. From the analysis with a consideration of a two-dimensional thermal diffusion in the substrate, when d increases from 1.5 to 5 mm, η is decreased from 90 to 55% for the case of $f = 9.8$ L/min. Moreover, as f decreases from 9.8 to 4.2 L/min, η is decreased to 57% at $d = 1$ mm and to 41% at $d = 5$ mm, indicating that the effusion velocity of the TPJ plays an important role in power transfer.

4. Applications of TPJ Annealing in Crystalline Si Formation

4.1 *Crystallization of a-Si films*

The TPJ annealing technique has been applied to the crystallization of a-Si films. For understanding phase transformation in millisecond time domain, an *in-situ* observation technique has been applied. Figure 6(a) shows examples of the transient reflectivity waveforms of a Si film measured during TPJ annealing with a d of 3.3 mm, a v of 770 mm/s, an f of 7.0 L/min and p values of (i) 1.89 kW where the Si film remains amorphous, (ii) 2.10 kW where a-Si film is transformed to crystalline and (iii) 2.10 kW where the Si film is in the crystalline phase throughout the measurement. The film annealed under condition (i) shows a gradually changing reflectivity because no phase transformation occurs by the annealing. Waveform (ii) until 9.6 ms is almost the same as waveform (i), but after 9.6 ms, waveform (ii) reflectivity suddenly decreases and completely differs from that of waveform (i). This is due to the phase transformation of the Si film from amorphous to crystalline. The crystallized film is again annealed and the obtained transient reflectivity is shown by (iii). Waveforms (ii) and (iii) are identical after 10.2 ms. The result indicates that the Si film annealed under condition (ii) is in the amorphous phase until 9.6 ms and is in the crystalline phase after 10.2 ms. From this result, we can confirm that the solid phase crystallization (SPC) of a-Si film occurs within the duration of 0.6 ms in this case. By combining this *in-situ* observation technique of phase transformation with the temperature measurement technique mentioned in §3, the crystallization temperature of a-Si films is determined. The measured surface temperature profile under condition (ii) is superimposed in Fig. 6(a). From this result, we can determine that SPC starts at 1221 K in this case. The transient reflectivity waveform obtained from an a-Si film annealed with a smaller d of 0.8 mm and the same v, f, and p of 770 mm/s, 7.0 L/min and 2.10 kW, respectively, is shown in Fig. 6(b). Surface temperature is also shown in the same graph. The waveform until 9.6 ms is almost identical to that of the trace (ii) in Fig. 6(a), which indicates that SPC occurs from 8.8 to 9.0 ms at 1278 K. Reflectivity rapidly increases to a value higher than 60% from 9.5 ms and decreases at 10.8 ms. Such a high reflectivity indicates the melting of the Si film.[2)] The a-Si film is firstly crystallized in the solid phase and the crystallized film is melted, and recrystallization from a molten Si occurs. From this result, we confirmed that the a-Si films annealed by TPJ are crystallized either in the solid or liquid phase depending on the condition. Note that SPC temperatures in Figs. 6(a) and 6(b) are different more than 50 K. This result suggests that SPC temperature may change depending on the annealing condition.

To confirm this, a-Si films were annealed under different conditions and the relationship between crystallization time

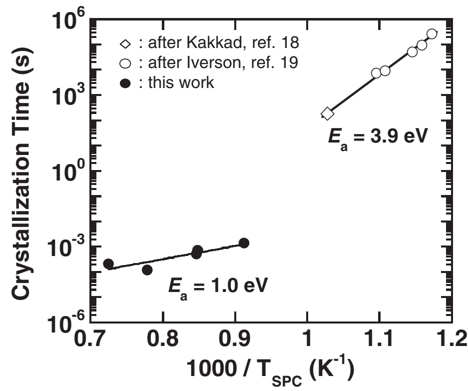

Fig. 7. Relationship between duration of phase transformation (crystallization time) and solid phase crystallization (SPC) temperature in Arrhenius plot. The results in our experiment and in conventional SPC experiments in the time range from 3 min to 90 h are plotted for comparison.

and SPC temperature was investigated. The result is shown as an Arrhenius plot in Fig. 7 along with the SPC experiments performed in the time domains of 3–5 min[18] and 2–80 h.[19] SPC temperature in the TPJ annealing increased from 1096 to 1284 K with decreasing crystallization time from 1.4 to 0.12 ms. The activation energy (E_a) of crystallization time in conventional SPC is consistently 3.9 eV. The SPC mechanism has been extensively studied by many researchers[20–22] and has been successfully used to explain the experimental results. On the other hand, E_a in our experiment is 1.0 eV, which is much smaller than the conventional E_a. So far, there is no clear explanation for this low E_a; we think that some effect enhancing the crystallization exists. Further investigation is needed to understand SPC mechanism in TPJ annealing.

For the evaluation of the crystallinity of SPC Si films, the Raman scattering spectra of 80-nm-thick Si films before and after TPJ annealing at different v values under a constant p of 2.40 kW, an f of 7.0 L/min and a d of 2.0 mm are measured and the results are shown in Fig. 8(a). By reducing v below 1000 mm/s, a sharp peak associated with crystalline Si transverse optical (TO) phonons appears at a wavenumber ranging from 515 to 518 cm^{-1}. By reducing v from 1000 to 550 mm/s, the full width at half maximum (FWHM) and position of the TO phonon peak are reduced from 19 to 11 cm^{-1} and increased from 515 to 518 cm^{-1}, respectively. These results indicate that the crystallinity of the Si films is improved by reducing v. Amorphous Si films are crystallized in the solid phase, and a higher temperature and a longer annealing duration have improved in crystallinity. The crystallization conditions of the a-Si films with respect to p and v are shown in Fig. 8(b). With increasing p, a-Si films crystallize at a higher v and the process window becomes larger. This indicates that the throughput of the TPJ crystallization technique is improved by an increase in p. However, film stripping is facilitated by a decrease in v to a certain value. Film stripping is frequently observed in conditions where the Si melts in our experiment. According to the transient reflectivity measurement, film stripping occurs during the solidification of a molten Si film. Similar phenomena, such as film stripping and agglomeration, have been reported in many crystallization techniques.[3–8] These

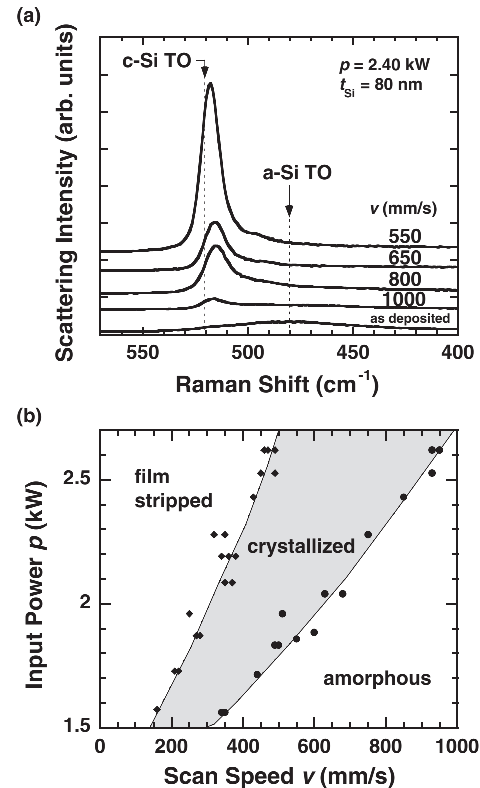

Fig. 8. (a) Raman scattering spectra obtained from 80-nm-thick Si films as-deposited and TPJ-treated under different v values ranging from 550 to 1000 mm/s and constant p of 2.40 kW, f of 7.0 L/min, d of 2.0 mm, and (b) crystallization conditions of a-Si films with respect to p and v.

phenomena originated either from the difference in thermal expansion coefficient between Si films and the underlying SiO_2 layer or the surface tension of a molten Si. Therefore, heating of the substrate, encapsulation or patterning of a-Si films might be effective for preventing this problem as reported in the literature.

4.2 *Thin-film transistor fabrication*

For the evaluation of the electrical characteristics of TPJ crystallized Si films, TFTs were fabricated by the following process.[23,24] 7×10^{20} cm^{-3}-phosphorus-doped a-Si films with a thickness of 25 nm were deposited by PECVD on quartz substrates and then patterned into islands to form source and drain regions. 20-nm-thick intrinsic a-Si films were deposited on the source/drain islands by PECVD of 50% SiH_4 diluted with H_2 at 150 °C. The TPJ crystallization was performed to crystallize the a-Si film and to activate the phosphorus atoms in source and drain regions, simultaneously. The intrinsic layer thickness was set at 20 nm to allow the diffusion of the impurities in the underlying doped Si film to the top intrinsic layer and the formation of good Ohmic contacts with Al electrodes. In the TPJ crystallization, p was varied from 1.86 to 2.29 kW at a constant f of 9.8 L/min, d of 2.0 mm and v of 700 mm/s. Under this condition, the a-Si films are crystallized in the solid phase. After etching the Si layer to an island shape, source and drain electrodes were formed by the evaporation of Al, followed by the deposition of a 100-nm-thick gate SiO_x film by molecular beam deposition from SiO powder in an oxygen radical atmosphere at room temperature. After the

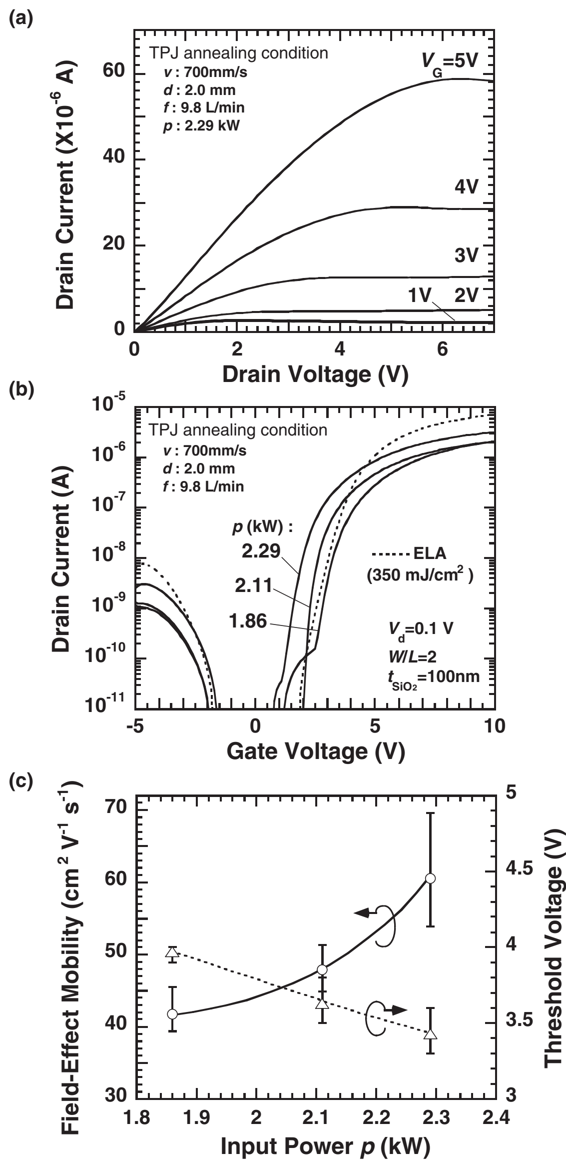

Fig. 9. Output (a) and transfer (b) characteristics of TFTs fabricated by TPJ technique. In (c), average μ_{FE} and V_{th} extracted from (b) are plotted as functions of p. The other annealing conditions are as follows: an f of 9.8 L/min, a d of 2.0 mm, and a v of 700 mm/s.

gate electrode formation by Al evaporation, high-pressure H_2O vapor annealing was performed at 260 °C and 1.3×10^6 Pa for 3 h to reduce defect states in the Si film and at the gate SiO_x/Si interface.[25–27] The maximum temperature throughout the fabrication process was 260 °C.

The fabricated TFTs show good electrical performance as seen in the output and transfer characteristics shown in Figs. 9(a) and 9(b), respectively. The transfer characteristic of a TFT fabricated in the same run by ELA for the a-Si crystallization is shown in Fig. 9(b) for comparison. The on-current of TPJ crystallized TFTs increase as p during the crystallization increases from 1.86 to 2.29 kW. The field-effect mobility (μ_{fe}) and threshold voltage (V_{th}) of the TFTs extracted from the transfer characteristics are shown in Fig. 9(c) as functions of p. The error bars indicate the maximum and minimum values obtained from three to eight transistors. Average μ_{fe} increases from 42 to 61 $cm^2 \cdot V^{-1} \cdot s^{-1}$ and V_{th} decreases from 4.0 to 3.4 V with increasing p from 1.86 to 2.29 kW. These results are in good agreement with an improvement in crystallinity by the increase in p. That is, the crystalline network with fewer defects is likely to be formed in higher-temperature crystallization. The TFT fabricated by ELA shows a high μ_{fe} of 160 $cm^2 \cdot V^{-1} \cdot s^{-1}$, as understood from a high on-current in the high-gate-voltage region. However, a V_{th} of 4.5 V is much higher than that of TPJ TFTs. This result suggests that the polycrystalline Si films prepared by ELA contain a higher density of trap states compared with those of TPJ films, presumably due to the high R_c on the order of 10^{10} K/s,[2] which is five orders of magnitude larger than that of TPJ annealing (see Tables I and II). From these results, we confirmed that the TPJ crystallization technique is applicable to the fabrication of TFTs.

4.3 Precipitation of nanocrystalline Si in SiO_x films

As for another way of forming Si crystals, we have applied TPJ annealing to Si-rich oxide [SiO_x ($x < 2$)] films. SiO_x films were formed on a quartz substrate by the vacuum evaporation of SiO powder with a thickness ranging from 401 to 911 nm. The Raman scattering spectra and atomic force microscopy (AFM) image obtained from a 401-nm-thick as-deposited SiO film are shown in Fig. 10(a). The Raman scattering spectrum is almost identical to that of the quartz substrate which is characterized by a broad peak at approximately 437 cm^{-1} and a relatively narrow peak at 497 cm^{-1} referred as D_1 peak.[28,29] The surface of the as-deposited SiO_x film is relatively smooth. By annealing the film with a p of 2.09 kW and a v of 700 mm/s, no significant change was observed in Raman scattering spectra; however, we found a change in surface morphology which is characterized by a uniformly dispersed nanosized spherical structure with a typical size of 10 nm in diameter. Also, we confirmed a clear change in film color from dark brown to yellow. By decreasing v to 600 mm/s, a sharp Raman scattering peak is observed at 518 cm^{-1}, which is identified as a crystalline Si TO phonon band, and larger nanosized spherical structures with the diameter of approximately 30 nm are observed as shown in Fig. 10(b). When a 911-nm-thick SiO_x film is annealed with a v of 300 mm/s, much larger Si crystalline spheres were formed as shown in Fig. 10(c). A very sharp Raman scattering peak at 520 cm^{-1} and huge spherical structures as large as 250 nm in diameter are observed in this sample.

The equilibrium composition of this system at a high temperature is Si and SiO, but it is Si and SiO_2 at room temperature, which means that SiO_x at room temperature is in a supersaturated condition. Therefore, heating and cooling of SiO_x results in phase separation into Si and SiO_2. It has been reported that nanocrystalline Si precipitates in SiO_x films when the films are annealed at a temperature as high as 1000 °C and at an annealing duration as long as 30 min.[30,31] In our experiment, the precipitation of Si nanocrystals has been observed at temperatures higher than 1467 K with an annealing duration of approximately 1.8 ms. This result suggests that phase separation in SiO_x films is promoted by a high annealing temperature. From the specimen annealed with a v of 700 mm/s, red photoluminescence was observed at room temperature with a peak wavelength of approximately 710 nm.

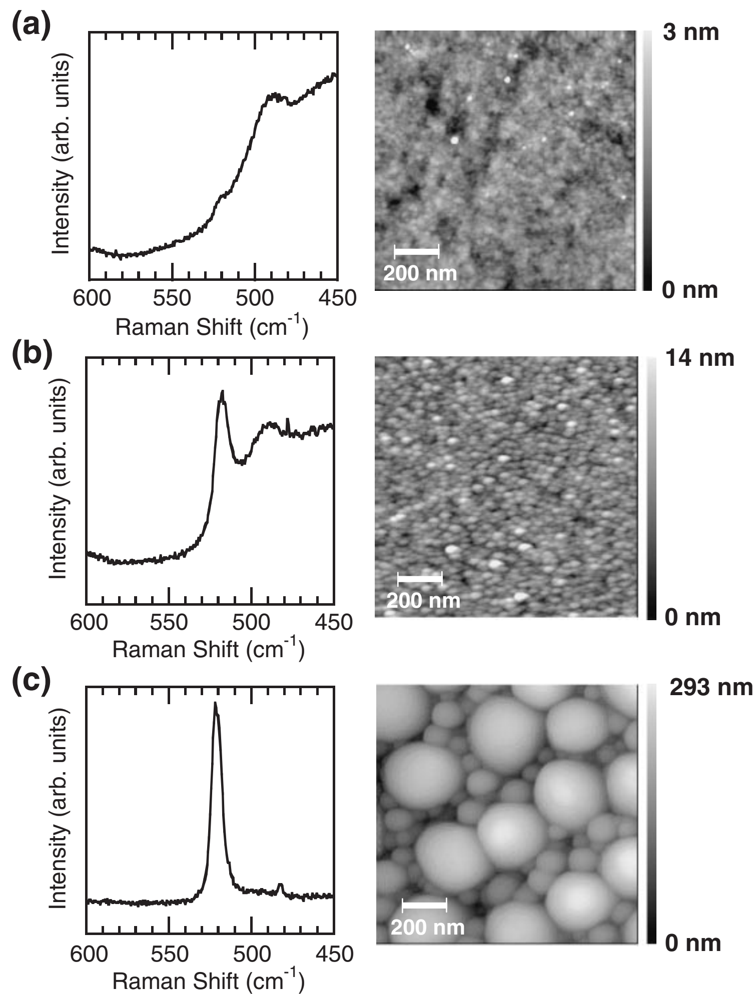

Fig. 10. Raman scattering spectra (left) and surface morphology observed by atomic force microscopy (AFM) (right) of (a) as-deposited SiO_x film and TPJ-annealed SiO_x films with a p of 2.09 kW and v values of (b) 600 and (c) 300 mm/s. The vertical gray scale bars at the right hand side of the AFM images indicate the full scale of the measured height.

5. Conclusions

An optical probe method enables us to measure transient temperature profiles generated in a quartz substrate during TPJ annealing with an accuracy of 30 K. By changing v, T_{max} and t_a changes simultaneously, whereas by changing d or f under constant v, T_{max} is controlled without significantly changing t_a. Accordingly, we can control T_{max} in the ranges of 960 to 1860 K with a typical t_a of $\sim$3 ms. Amorphous Si films annealed by TPJ are crystallized either by SPC or liquid phase crystallization. When the films are heated to a temperature higher than the melting point, a-Si is firstly crystallized in a solid phase followed by melting and resolidification. It was found that the E_a of crystallization time in a rapid SPC is 1.0 eV, which is much smaller than that in SPC with a time domain longer than 3 min. The application of TPJ to the fabrication of TFTs has been demonstrated with a μ_{FE} of 61 $cm^2 \cdot V^{-1} \cdot s^{-1}$ and a V_{th} of 3.4 V, respectively. The precipitation of nanocrystalline Si with a size ranging from 10 to 250 nm in SiO_x films has been observed by annealing the films using a TPJ at temperatures higher than 1467 K. Rapid thermal annealing using TPJ is quite useful for the formation of crystalline Si in millisecond time domain.

Acknowledgements

The authors would like to acknowledge Professor Sameshima of Tokyo University of Agriculture and Technology for TFT fabrication. A part of this work was supported by the Industrial Technology Research Grant Program in 2005 from the New Energy and Industrial Technology Development Organization (NEDO) of Japan.

1) T. Sameshima and S. Usui: J. Appl. Phys. **70** (1991) 1281.
2) S. Higashi and T. Sameshima: Jpn. J. Appl. Phys. **40** (2001) 480.
3) R. A. Lemons, M. A. Bosch, A. H. Dayem, J. K. Grogan and P. M. Mankiewich: Appl. Phys. Lett. **40** (1982) 469.
4) S. Kawamura, J. Sakurai, M. Nakano and M. Takagi: Appl. Phys. Lett. **40** (1982) 394.
5) D. J. Wouters and H. E. Maes: J. Appl. Phys. **66** (1989) 900.
6) A. Doi, T. Asakawa and S. Namba: Jpn. J. Appl. Phys. **28** (1989) L128.
7) A. Hara, F. Takeuchi, M. Takei, K. Suga, K. Yoshino, M. Chida, Y. Sano and N. Sasaki: Jpn. J. Appl. Phys. **41** (2002) L311.
8) N. Sotani, I. Hasegawa, D. Ide, T. Nohda and K. Yamano: Jpn. J. Appl. Phys. **44** (2005) 21.
9) T. Sameshima and K. Ozaki: Jpn. J. Appl. Phys. **39** (2000) L651.
10) T. Sameshima, Y. Kaneko and N. Andoh: Appl. Phys. A **73** (2001) 419.
11) Y. Kaneko, N. Andoh and T. Sameshima: Jpn. J. Appl. Phys. **41**

(2002) L913.
12) H. Kaku, S. Higashi, H. Taniguchi, H. Murakami and S. Miyazaki: Appl. Surf. Sci. **244** (2005) 8.
13) S. Higashi, H. Kaku, H. Taniguchi, H. Murakami and S. Miyazaki: Thin Solid Films **487** (2005) 122.
14) K. C. Hsu, K. Etemadi and E. Pfender: J. Appl. Phys. **54** (1983) 1293.
15) J. H. Wray and J. T. Neu: J. Opt. Soc. Am. **59** (1969) 774.
16) T. Okada, S. Higashi, H. Kaku, H. Murakami and S. Miyazaki: Dig. Tech. Pap. AM-LCD 05, Kanazawa, Japan, July 6–8, 2005, p. 171.
17) T. Okada, S. Higashi, H. Kaku, N. Koba, H. Murakami and S. Miyazaki: Proc. Int. Symp. Dry Process, Jeju, Korea, November 28–30, 2005, p. 405.
18) R. Kakkad, J. Smith, W. S. Lau, S. J. Fonash and R. Kerns: J. Appl. Phys. **65** (1989) 2069.
19) R. B. Iverson and R. Reif: J. Appl. Phys. **62** (1987) 1675.
20) D. Turnbull and J. C. Fisher: J. Chem. Phys. **17** (1949) 71.
21) K. F. Kelton, A. L. Greer and C. V. Thompson: J. Chem. Phys. **79** (1983) 6261.
22) F. G. Shi: J. Appl. Phys. **76** (1994) 5149.
23) S. Higashi, H. Kaku, H. Murakami, S. Miyazaki, M. Asami, H. Watakabe, N. Ando and T. Sameshima: Dig. Tech. Pap. AM-LCD 04, Tokyo Japan, August 25–27, 2004, p. 179.
24) S. Higashi, H. Kaku, H. Murakami, S. Miyazaki, H. Watakabe, N. Ando and T. Sameshima: Jpn. J. Appl. Phys. **44** (2005) L108.
25) T. Sameshima and M. Satoh: Jpn. J. Appl. Phys. **36** (1997) L687.
26) K. Asada, K. Sakamoto, T. Watanabe, T. Sameshima and S. Higashi: Jpn. J. Appl. Phys. **39** (2000) 3883.
27) T. Sameshima, K. Sakamoto and K. Asada: Appl. Phys. A **69** (1999) 221.
28) F. L. Galeener: Phys. Rev. B **19** (1979) 4292.
29) F. L. Galeener: J. Non-Cryst. Solids **49** (1982) 53.
30) D. J. DiMaria, J. R. Kirtley, E. J. Pakulis, D. W. Dong, T. S. Kuan, F. L. Pesavento, T. N. Theis, J. A. Cutro and S. D. Brorson: J. Appl. Phys. **56** (1984) 401.
31) D. Nesheve, C. Rapits, A. Perakis, I. Bineva, Z. Aneva, Z. Lezi, S. Alexandrova and H. Hofmeister: J. Appl. Phys. **92** (2002) 4678.